Table 1
Cytotoxic activity and ROS inducing activity of RID-SB8 in fifteen cancer cell lines and two primary normal epithelial cell lines.

Cell lines	IC_{50} (μM)	ROS inducing activity (μM)	Cell lines	IC_{50} (μM)	ROS inducing activity (μM)
MCF-7	3.04	4.12	NCI-H226	11.7	19.2
MDA-MB-231	2.81	3.15	NCI-H23	6.61	8.11
SK-OV3	5.62	3.19	PC-3	12.1	18.1
SF539	2.10	1.84	DU-145	15.4	20.7
SF295	4.80	2.50	RXF	4.65	6.25
SNB78	4.57	8.65	ACHN	5.63	4.46
SNB75	4.83	10.16			
HT-29	3.88	8.14	HMEC	23.2	>32.0
HCC2998	4.12	8.45	RPTEC	21.2	>32.0

treatment with tamoxifen did not induce the translocation of AIF even at high concentration (20 μM).

To investigate the functional involvement of AIF translocation in the RID-SB8-induced anticancer effect, knockdown of AIF in SF539 cells was performed using AIF siRNA. The effect of two AIF siRNA was confirmed by western blotting, the amount of AIF protein was markedly reduced by treatment of both of the two AIF siRNA for 24 h (Fig. 6D). AIF siRNA-treated SF539 cells showed lower sensitivity to RID-SB8 than control siRNA-treated cells in the cell viability assay (Fig. 6E). These results suggested that AIF played an important role in RID-SB8-induced apoptosis.

3.6. RID-SB8-induced apoptosis is attributed to induction of ROS

As known, ROS are involved in both caspase-dependent and caspase-independent cell death. Therefore, we determined whether ROS are required for RID-SB8-induced apoptosis. First, we examined whether RID-SB8 induced ROS in SF539 cells using a ROS probe, CM-H_2DCFDA. As shown in Fig. 7A, treatment with RID-SB8 for 2 h resulted in an increase in ROS level in a dose-dependent manner. Moreover, the ROS generation was completely inhibited by treatment with a ROS scavenger, *N*-acetyl-L-cysteine (NAC) (Fig. 7A). Next, we evaluated the involvement of ROS in the progression of apoptosis induced by RID-SB8. Pretreatment with NAC (10 mM) for 1 h effectively protected against loss of cell viability after treatment with RID-SB8 (Fig. 7B). Similarly, the population of apoptotic cells caused by RID-SB8 was significantly reduced by pretreatment with NAC (Fig. 7C). As expected, pretreatment with NAC also attenuated RID-SB8-induced loss of $\Delta\Psi_m$ (Fig. 7D), caspase activation and translocation of AIF (Fig. 7E). On the other hand, tamoxifen showed no ROS induction activity in SF539 cells until the concentration was increased to 40 μM

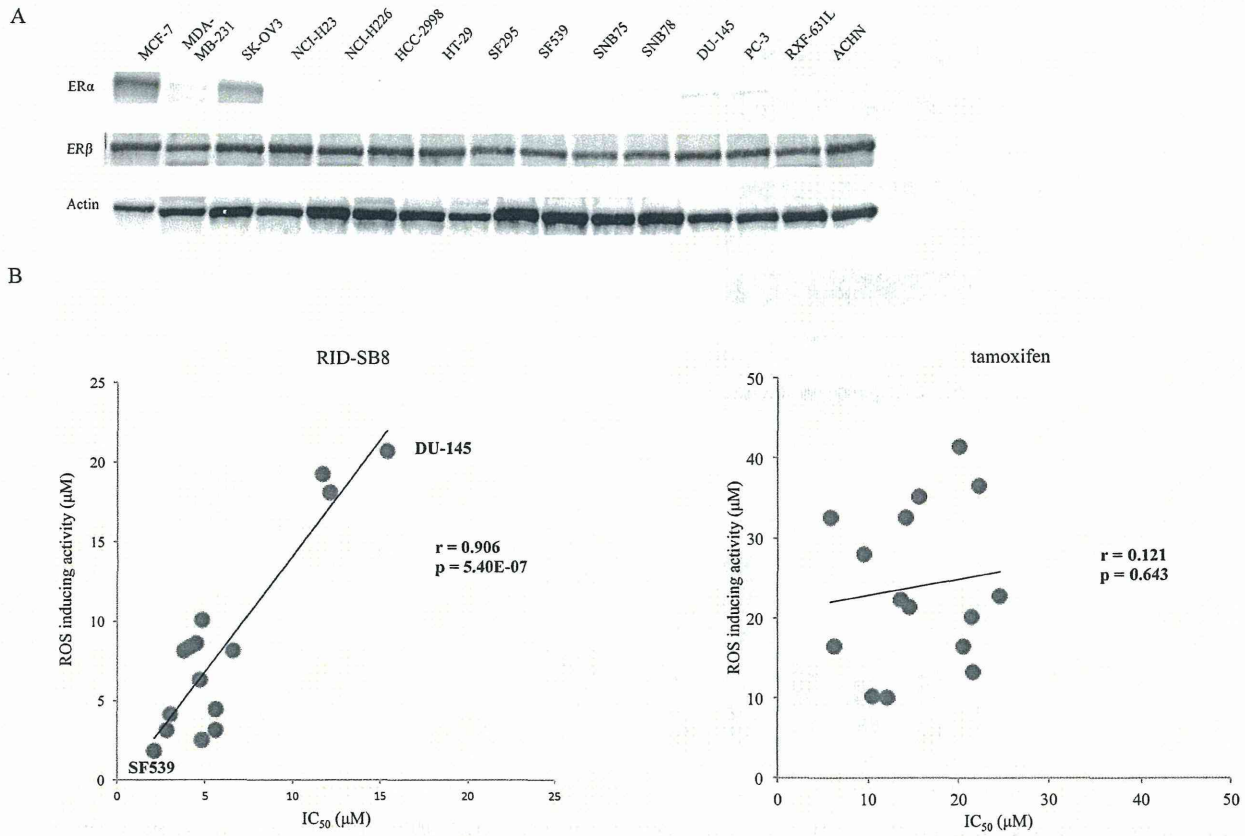

Fig. 8. (A) Correlation between cytotoxic activity and ROS inducing activity of RID-SB8 across fifteen human cancer cell lines. (A) Cell lysates were prepared from fifteen human cancer cell lines and analyzed by Western blotting. (B and C) The concentration at which compounds could induce 2-fold generation of ROS compared to control was used to evaluate the ROS inducing activity. Scatter plots of fifteen human cell cell lines (described in Section 2, *Cell lines and cell culture*) showing signficant correlation between cytotoxic activity and ROS inducing activity of RID-SB8 (Person correlation coefficients: $r = 0.906$, $p < 0.01$), but not tamoxifen (Person correlation coefficients: $r = 0.121$).

(Fig. 7F). Moreover, pretreatment with NAC did not eliminate the cytotoxic effect of tamoxifen on SF539 cells (Fig. 7G). These results indicated that the induction of ROS generation is critically important for RID-SB8-induced apoptosis *via* the mitochondrial pathway, but not for cell death induced by tamoxifen.

3.7. Correlation between cytotoxic activity and ROS inducing activity of RID-SB8 across fifteen human cancer cell lines

To further confirm the importance of ROS generation in RID-SB8-induced apoptosis, we examined the correlation between cytotoxic activity and ROS inducing activity using fifteen human cancer cell lines. First, we characterized the expression status of ERα and ERβ in these cell lines. Expectedly, MCF-7 and SK-OV3 highly expressed ERα, whereas others including SF539 exhibited very weak or no expression. In contrast, ERβ is ubiquitously expressed across all of the fifteen cell lines. Then, we examined the cytotoxic activity and the ROS inducing activity in each of the fifteen cell lines. The values of IC_{50} and the concentration required to induce 2-fold ROS generation over fifteen cell lines were summarized in Table 1. For example, RID-SB8 exhibited the strongest activity in cytotoxic effect with an IC_{50} of 2.10 μM and ROS inducing effect at a concentration of 1.84 μM, in SF539 cells (Table 1). In contrast, RID-SB8 showed the weakest activities in prostate cancer DU-145 with an IC_{50} of 15.4 μM and ROS inducing effect at a concentration of 20.7 μM, respectively (Table 1). Our analysis revealed a statistically significant correlation ($r = 0.908$ and $p < 0.01$) between these two activities of RID-SB8 across fifteen cancer cell lines (Fig. 8A). On the other hand, tamoxifen showed no correlation between these two activities in these cell lines (Fig. 8B). Taken together, our results suggested that there is a causal relationship between the cytotoxic activity and ROS inducing activity of RID-SB8.

3.8. RID-SB8 preferentially induced cell death in cancer cells

To characterize the selectivity of ROS-inducing activity and the cytotoxicity of RID-SB8 in cancer cells, we examined the ROS level and the viability in normal cells and compared them with those of malignant counterparts. As shown in Fig. 9A, breast cancer cells such as MCF-7 and MDA-MB-231 exhibited high sensitivity to RID-SB8 (IC_{50} = 3.04 μM and 2.81 μM, respectively), whereas their normal counterparts, HMEC, exhibited resistance by > 7-fold (IC_{50} = 23.2 μM). Similar results were obtained in renal cancer RXF-631L and ACHN cells and their normal counterparts, RPTEC. As for the ROS level, all of four cancer cell lines exhibited a strong induction of ROS, whereas their normal counterparts did not exhibit significant ROS induction after exposure to RID-SB8 (16 μM). Moreover, the basal ROS levels in cancer cells were significantly higher than those in normal cells, except for MCF-7 cells. From these results, we concluded that RID-SB8 selectively induced cell death in cancer cells and that the selectivity might be due to the higher basal ROS level and induction of ROS in cancer cells.

4. Discussion

In the present study, we synthesized a tamoxifen derivative, RID-SB8, capable of producing a strong anticancer effect. This effect is independent of ERα, which is the primary target for tamoxifen. We also demonstrated that RID-SB8 exerts selective cytotoxic activity *via* ROS generation in cancer cells, resulting in the loss of mitochondrial membrane potential and activation of caspase-dependent and -independent apoptosis pathways. From these results we concluded that RID-SB8 is a novel anticancer lead compound with a different mode of action to tamoxifen.

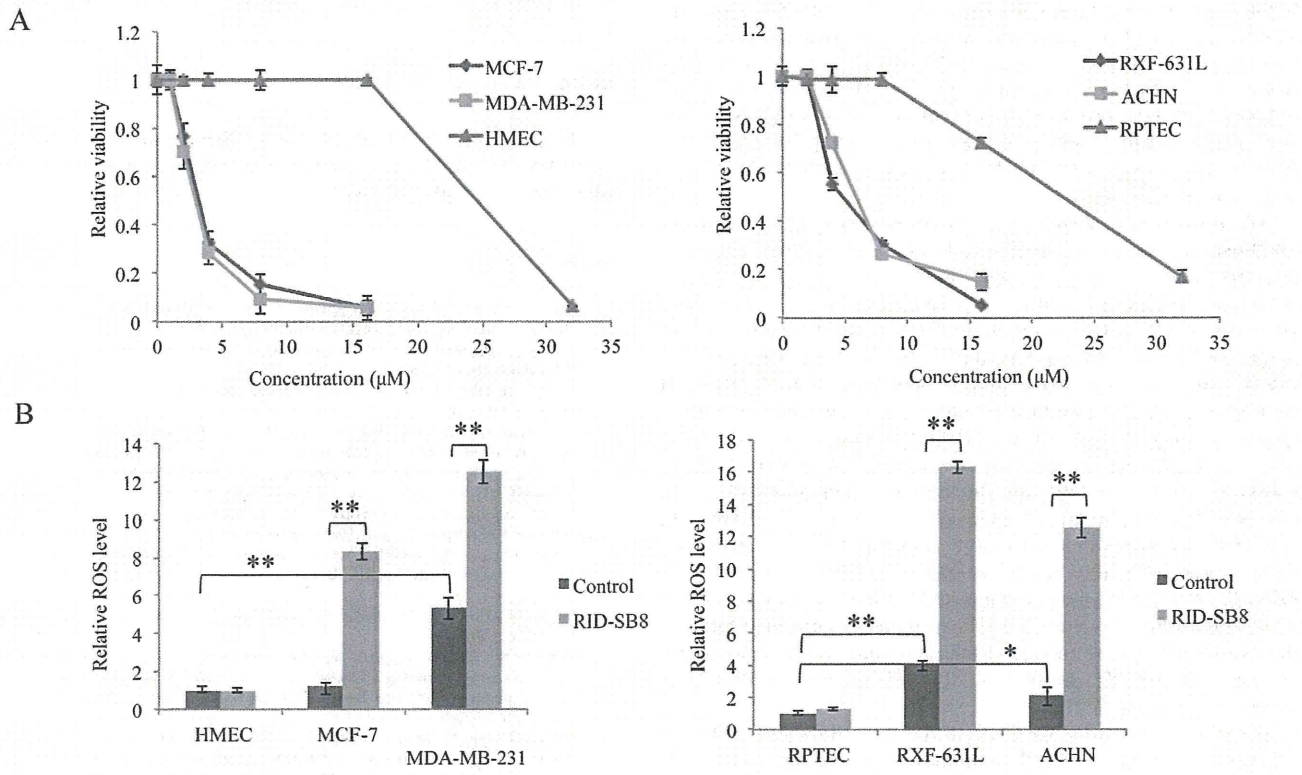

Fig. 9. Selective induction of ROS and cell death in cancer cells. (A) Cell viability after treatment with RID-SB8 for 24 h was determined by WST-8 asssay. (B) Cells growing in black 96-well plate were exposed to RID-SB8 for 2 h. Subsequently, cells were loaded with CM-H_2DCFDA for 30 min, followed by dectection using a microplate reader. All the results except for (E) represent the means ± SD from three independent experiments. Differences with $p < 0.05$ (*) or $p < 0.01$ (**) are considered statistically significant.

We previously reported a novel total synthetic method for tamoxifen and its derivatives, named as Ridaifens. Among them, we identified RID-SB8, which has no ERα-binding activity and potent anticancer activity [11]. In the present study, in two ERα-positive and thirteen ERα-negative cancer cells lines, the cytotoxic activity of RID-SB8 was observed regardless of ERα expression, indicating that RID-SB8 exerted anticancer activity in an ERα-independent manner (Table 1). This hypothesis was further supported by a viability assay in ERα knockdown MCF-7. In ERα siRNA-treated MCF-7, the sensitivity to RID-SB8 remained unchanged (Fig. 3C). From these results, we concluded that anticancer activity of RID-SB8 is independent of ERα. ERβ is thought to have antiproliferative and proapoptotic functions while ERα is thought to promote the expression of genes involved in cell survival and proliferation [40,41]. In regard to ERβ, its expression has been shown in various types of cancer including breast cancer [42], prostate cancer [43,44], colon cancer [45], ovarian cancer [46], glioma cancer [47], renal cancer [48] and lung cancer [49]. In the present study, we demonstrated that ERβ is ubiquitously expressed across the fifteen cell lines regardless of their sensitivity to RID-SB8, suggesting that ERβ has nothing to do with the anticancer mechanism of RID-SB8.

ROS are known as active mediators in the regulation of cell death, including caspase-dependent and caspase-independent pathways *via* mitochondrial dysfunction [50–52]. In the present study we showed that RID-SB8 exerted mitochondrial dysfunction and caspase-dependent and independent apoptosis by inducing ROS. Actually, we observed the significant correlation between the cytotoxic activity and ROS inducing activity across fifteen cancer cell lines (Fig. 8A). Furthermore, the concentration needed to cause cell death in each cell line was similar to that needed for ROS induction (Fig. 8B), which further confirmed the importance of ROS generation in the anticancer activity of RID-SB8. In several reports, tamoxifen was shown to induce ROS leading to apoptosis [53,54]. In our present study, tamoxifen certainly induced ROS in all of the fifteen cancer cell lines tested; however, in most cell lines the concentration required to induce ROS was much higher than that needed to suppress cell viability by 50%. At 40 μM, tamoxifen induced ROS generation, but pretreatment with NAC could not prevent the cytotoxic effect of tamoxifen in SF539 cells (Fig. 7G). These results suggested that ROS is not the main factor in the cell death induced by tamoxifen.

We previously reported that one of the RIDs, RID-B, induced apoptosis in human leukemia cell line Jurkat [55]. However, apoptosis induced by RID-B was not suppressed by the radical scavenger, 3,3,5,5-tetramethyl-1-pyrolline-N-oxide (TMPO), suggesting that ROS is not a fundamental factor in RID-B-induced cell death, or in tamoxifen-induced cell death. COMPARE analysis [35,36] revealed that RID-B had a significant correlation with tamoxifen ($r = 0.69$) (unpublished data). Moreover, RID-B exhibited strong affinity to ER ($IC_{50} = 52.4$ nM) similar to tamoxifen ($IC_{50} = 21.1$ nM). These observations indicate a similar mode of action for RID-B as for tamoxifen, including ER-dependent effects. In contrast, RID-SB8 did not correlate with tamoxifen ($r = 0.318$), and exhibited no ERα binding activity ($IC_{50} > 10$ μM) [11], suggesting a different mechanism to that of tamoxifen. All of these properties of RID-SB8 are probably due to the loss of the phenyl group from the C-2 position in the ethylenic bond. We previously demonstrated that this phenyl group was indispensable in binding to ER, while it was not required for ROS-dependent RID-SB8-induced apoptosis observed in our present study.

In the present study, we showed that RID-SB8 exerts selective cytotoxic activity *via* ROS generation in cancer cells. We demonstrated that three of four cancer cell lines exhibited higher basal level of ROS compared to normal counterparts. Since cancer cells usually have a relatively high basal ROS level [56], a slight increase in ROS may push the cellular ROS level over the threshold, leading to cell death. In contrast, normal cells with low basal ROS level can tolerate the oxidative stress. Of note, we further demonstrated that cancer cells exhibited a strong induction of ROS upon treatment with RID-SB8, whereas their normal counterparts did not. It was reported that a ROS inducer, piperlongumine, selectively induced ROS in cancer cells and the consequent selective killing of cancer cells are attributed to the cancer genotype of transformed cells [32]. Although the mechanism remains to be elucidated, we suspect that cancer specific induction of ROS plays an important role in anticancer activity of RID-SB8. Meanwhile, it was reported that excessive ROS production can increase inflammation and induce an epigenetic switch, and ROS associated signaling pathways involved in tumor progression, especially in epithelial-mesenchymal transition (EMT) [57,58]. To elucidate the effect of RID-SB8-induced ROS production on tumor progression and EMT, further studies using *in vivo* models are needed.

In summary, we synthesized a novel tamoxifen-derivative, RID-SB8, which exerts a cancer-cell-selective killing effect *via* the generation of ROS, dysfunction of mitochondrial membrane potential, and induction of caspase-dependent and -independent apoptosis. Therefore, we concluded that RID-SB8 could be a novel anticancer lead compound that preferentially kills cancer cells by targeting the ROS stress–response pathway.

Grant support

This work was supported by Health Labour Sciences Research Grant from The Ministry of Health Labour and Welfare to IS and SD (11103425); Grants-in-Aid for Scientific Research (A) from Japan Society for the Promotion of Science to TY and SD (22240092) and Grant-in-Aid for Scientific Research on Priority Areas from the Ministry of Education, Culture, Sports, Science and Technology to TY and SD (221S0001).

Acknowledgment

We thank Ms. K. Yamazaki, Ms. Y. Nishimura, Ms. M. Okamura and Ms. N. Tamaki for technical assistance and Dr. Akinobu Akatsuka for helpful discussions.

References

[1] Jordan VC. Molecular mechanisms of antiestrogen action in breast cancer. Breast Cancer Research and Treatment 1994;31:41–52.
[2] Grainger DJ, Metcalfe JC. Tamoxifen: teaching an old drug new tricks? Nature Medicine 1996;2:381–5.
[3] Catherino WH, Jordan VC. A risk–benefit assessment of tamoxifen therapy. Drug Safety 1993;8:381–97.
[4] Beekman JM, Allan GF, Tsai SY, Tsai MJ, O'Malley BW. Transcriptional activation by the estrogen receptor requires a conformational change in the ligand binding domain. Molecular Endocrinology 1993;7:1266–74.
[5] Rochefort H, Borgna JL, Evans E. Cellular and molecular mechanism of action of antiestrogens. Journal of Steroid Biochemistry 1983;19:69–74.
[6] Watts CK, Sweeney KJ, Warlters A, Musgrove EA, Sutherland RL. Antiestrogen regulation of cell cycle progression and cyclin D1 gene expression in MCF-7 human breast cancer cells. Breast Cancer Research and Treatment 1994; 31:95–105.
[7] Mandlekar S, Kong AN. Mechanisms of tamoxifen-induced apoptosis. Apoptosis 2001;6:469–77.
[8] Obrero M, Yu DV, Shapiro DJ. Estrogen receptor-dependent and estrogen receptor-independent pathways for tamoxifen and 4-hydroxytamoxifen-induced programmed cell death. The Journal of Biological Chemistry 2002; 277:45695–703.
[9] Shiina I, Sano Y, Nakata K, Kikuchi T, Sasaki A, Ikekita M, et al. Synthesis and pharmacological evaluation of the novel pseudo-symmetrical tamoxifen derivatives as anti-tumor agents. Biochemical Pharmacology 2008;75:1014–26.
[10] Shiina I, Sano Y, Nakata K, Kikuchi T, Sasaki A, Ikekita M, et al. Synthesis of the new pseudo-symmetrical tamoxifen derivatives and their anti-tumor activity. Bioorganic & Medicinal Chemistry Letters 2007;17:2421–4.

[11] Guo WZ, Wang Y, Umeda E, Shiina I, Dan S, Yamori T. Search for novel anti-tumor agents from Ridaifens using JFCR39, a panel of human cancer cell lines. Biological & Pharmaceutical Bulletin 2013;36:1008–16.
[12] Henry-Mowatt J, Dive C, Martinou JC, James D. Role of mitochondrial membrane permeabilization in apoptosis and cancer. Oncogene 2004;23: 2850–60.
[13] van Gurp M, Festjens N, van Loo G, Saelens X, Vandenabeele P. Mitochondrial intermembrane proteins in cell death. Biochemical and Biophysical Research Communications 2003;304:487–97.
[14] Castedo M, Macho A, Zamzami N, Hirsch T, Marchetti P, Uriel J, et al. Mitochondrial perturbations define lymphocytes undergoing apoptotic depletion in vivo. European Journal of Immunology 1995;25:3277–84.
[15] Zamzami N, Marchetti P, Castedo M, Decaudin D, Macho A, Hirsch T, et al. Sequential reduction of mitochondrial transmembrane potential and generation of reactive oxygen species in early programmed cell death. The Journal of Experimental Medicine 1995;182:367–77.
[16] Marchetti P, Susin SA, Decaudin D, Gamen S, Castedo M, Hirsch T, et al. Apoptosis-associated derangement of mitochondrial function in cells lacking mitochondrial DNA. Cancer Research 1996;56:2033–8.
[17] Li P, Nijhawan D, Budihardjo I, Srinivasula SM, Ahmad M, Alnemri ES, et al. Cytochrome c and dATP-dependent formation of Apaf-1/caspase-9 complex initiates an apoptotic protease cascade. Cell 1997;91:479–89.
[18] Liu X, Kim CN, Yang J, Jemmerson R, Wang X. Induction of apoptotic program in cell-free extracts: requirement for dATP and cytochrome *c*. Cell 1996; 86:147–57.
[19] Leist M, Jaattela M. Four deaths and a funeral: from caspases to alternative mechanisms. Nature Reviews Molecular cell biology 2001;2:589–98.
[20] Strasser A, O'Connor L, Dixit VM. Apoptosis signaling. Annual Review of Biochemistry 2000;69:217–45.
[21] Kaufmann SH, Desnoyers S, Ottaviano Y, Davidson NE, Poirier GG. Specific proteolytic cleavage of poly(ADP-ribose) polymerase: an early marker of chemotherapy-induced apoptosis. Cancer Research 1993;53: 3976–85.
[22] Los M, Wesselborg S, Schulze-Osthoff K. The role of caspases in development, immunity, and apoptotic signal transduction: lessons from knockout mice. Immunity 1999;10:629–39.
[23] Sakahira H, Enari M, Nagata S. Cleavage of CAD inhibitor in CAD activation and DNA degradation during apoptosis. Nature 1998;391:96–9.
[24] Joza N, Susin SA, Daugas E, Stanford WL, Cho SK, Li CY, et al. Essential role of the mitochondrial apoptosis-inducing factor in programmed cell death. Nature 2001;410:549–54.
[25] Cregan SP, Dawson VL, Slack RS. Role of AIF in caspase-dependent and caspase-independent cell death. Oncogene 2004;23:2785–96.
[26] Susin SA, Lorenzo HK, Zamzami N, Marzo I, Snow BE, Brothers GM, et al. Molecular characterization of mitochondrial apoptosis-inducing factor. Nature 1999;397:441–6.
[27] Fleury C, Mignotte B, Vayssiere JL. Mitochondrial reactive oxygen species in cell death signaling. Biochimie 2002;84:131–41.
[28] Simon HU, Haj-Yehia A, Levi-Schaffer F. Role of reactive oxygen species (ROS) in apoptosis induction. Apoptosis 2000;5:415–8.
[29] Circu ML, Aw TY. Reactive oxygen species, cellular redox systems, and apoptosis. Free Radical Biology & Medicine 2010;48:749–62.
[30] Chan WH, Wu CC, Yu JS. Curcumin inhibits UV irradiation-induced oxidative stress and apoptotic biochemical changes in human epidermoid carcinoma A431 cells. Journal of Cellular Biochemistry 2003;90:327–38.
[31] Trachootham D, Alexandre J, Huang P. Targeting cancer cells by ROS-mediated mechanisms: a radical therapeutic approach? Nature Reviews Drug Discovery 2009;8:579–91.
[32] Raj L, Ide T, Gurkar AU, Foley M, Schenone M, Li X, et al. Selective killing of cancer cells by a small molecule targeting the stress response to ROS. Nature 2011;475:231–4.
[33] Yamori T. Panel of human cancer cell lines provides valuable database for drug discovery and bioinformatics. Cancer Chemotherapy and Pharmacology 2003;52(Suppl. 1):S74–9.
[34] Nakatsu N, Nakamura T, Yamazaki K, Sadahiro S, Makuuchi H, Kanno J, et al. Evaluation of action mechanisms of toxic chemicals using JFCR39, a panel of human cancer cell lines. Molecular Pharmacology 2007;72: 1171–80.
[35] Dan S, Tsunoda T, Kitahara O, Yanagawa R, Zembutsu H, Katagiri T, et al. An integrated database of chemosensitivity to 55 anticancer drugs and gene expression profiles of 39 human cancer cell lines. Cancer Research 2002; 62:1139–47.
[36] Kong D, Yamori T, Kobayashi M, Duan H. Antiproliferative and antiangiogenic activities of smenospongine, a marine sponge sesquiterpene aminoquinone. Marine Drugs 2011;9:154–61.
[37] Ohashi Y, Iijima H, Yamaotsu N, Yamazaki K, Sato S, Okamura M, et al. AMF-26, a novel inhibitor of the Golgi system, targeting ADP-ribosylation factor 1 (Arf1) with potential for cancer therapy. Journal of Biological Chemistry 2012;287: 3885–97.
[38] Kong D, Okamura M, Yoshimi H, Yamori T. Antiangiogenic effect of ZSTK474, a novel phosphatidylinositol 3-kinase inhibitor. European Journal of Cancer 2009;45:857–65.
[39] Eglen RM. Enzyme fragment complementation: a flexible high throughput screening assay technology. Assay and Drug Development Technologies 2002;1:97–104.
[40] Thomas C, Gustafsson JA. The different roles of ER subtypes in cancer biology and therapy. Nature Reviews Cancer 2011;11:597–608.
[41] Gallo D, De Stefano I, Grazia Prisco M, Scambia G, Ferrandina G. Estrogen receptor beta in cancer: an attractive target for therapy. Current Pharmaceutical Design 2012;18:2734–57.
[42] Vladusic EA, Hornby AE, Guerra-Vladusic FK, Lakins J, Lupu R. Expression and regulation of estrogen receptor beta in human breast tumors and cell lines. Oncology Reports 2000;7:157–67.
[43] McPherson SJ, Hussain S, Balanathan P, Hedwards SL, Niranjan B, Grant M, et al. Estrogen receptor-beta activated apoptosis in benign hyperplasia and cancer of the prostate is androgen independent and TNFalpha mediated. Proceedings of the National Academy of Sciences of the United States of America 2010;107:3123–8.
[44] Mak P, Leav I, Pursell B, Bae D, Yang X, Taglienti CA, et al. ERbeta impedes prostate cancer EMT by destabilizing HIF-1alpha and inhibiting VEGF-mediated snail nuclear localization: implications for Gleason grading. Cancer Cell 2010;17:319–32.
[45] Fang YJ, Wang GQ, Lu ZH, Zhang LY, Pan ZZ, Zhou ZW, et al. Effects of tamoxifen on apoptosis and matrix metalloproteinase-7 expression in estrogen receptor beta-positive colonic cancer cell line HT-29. Ai Zheng 2008;27:1172–6.
[46] Lau KM, Mok SC, Ho SM. Expression of human estrogen receptor-alpha and -beta, progesterone receptor, and androgen receptor mRNA in normal and malignant ovarian epithelial cells. Proceedings of the National Academy of Sciences of the United States of America 1999;96:5722–7.
[47] Sareddy GR, Nair BC, Gonugunta VK, Zhang QG, Brenner A, Brann DW, et al. Therapeutic significance of estrogen receptor beta agonists in gliomas. Molecular Cancer Therapeutics 2012;11:1174–82.
[48] Yu CP, Ho JY, Huang YT, Cha TL, Sun GH, Yu DS, et al. Estrogen inhibits renal cell carcinoma cell progression through estrogen receptor-beta activation. PLoS ONE 2013;8:e56667.
[49] Pietras RJ, Weinberg OK. Antiangiogenic steroids in human cancer therapy. Evidence-Based Complementary and Alternative Medicine 2005;2:49–57.
[50] Jacobson MD. Reactive oxygen species and programmed cell death. Trends in Biochemical Sciences 1996;21:83–6.
[51] Guenal I, Sidoti-de Fraisse C, Gaumer S, Mignotte B. Bcl-2 and Hsp27 act at different levels to suppress programmed cell death. Oncogene 1997;15:347–60.
[52] Kang YH, Yi MJ, Kim MJ, Park MT, Bae S, Kang CM, et al. Caspase-independent cell death by arsenic trioxide in human cervical cancer cells: reactive oxygen species-mediated poly(ADP-ribose) polymerase-1 activation signals apoptosis-inducing factor release from mitochondria. Cancer Research 2004; 64:8960–7.
[53] Gundimeda U, Chen ZH, Gopalakrishna R. Tamoxifen modulates protein kinase C via oxidative stress in estrogen receptor-negative breast cancer cells. Journal of Biological Chemistry 1996;271:13504–14.
[54] Ferlini C, Scambia G, Marone M, Distefano M, Gaggini C, Ferrandina G, et al. Tamoxifen induces oxidative stress and apoptosis in oestrogen receptor-negative human cancer cell lines. British Journal of Cancer 1999;79:257–63.
[55] Nagahara Y, Shiina I, Nakata K, Sasaki A, Miyamoto T, Ikekita M. Induction of mitochondria-involved apoptosis in estrogen receptor-negative cells by a novel tamoxifen derivative, ridaifen-B. Cancer Science 2008;99:608–14.
[56] Sun X, Ai M, Wang Y, Shen S, Gu Y, Jin Y, et al. Selective induction of tumor cell apoptosis by a novel P450-mediated reactive oxygen species (ROS) inducer methyl 3-(4-nitrophenyl) propiolate. Journal of Biological Chemistry 2013; 288:8826–37.
[57] Rosanna DP, Salvatore C. Reactive oxygen species, inflammation, and lung diseases. Current Pharmaceutical Design 2012;18:3889–900.
[58] Giannoni E, Parri M, Chiarugi P. EMT and oxidative stress: a bidirectional interplay affecting tumor malignancy. Antioxidants and Redox Signalling 2012;16:1248–63.

European Journal of Medicinal Chemistry 71 (2014) 290–305

Contents lists available at ScienceDirect

European Journal of Medicinal Chemistry

journal homepage: http://www.elsevier.com/locate/ejmech

Original article

A novel tamoxifen derivative, ridaifen-F, is a nonpeptidic small-molecule proteasome inhibitor

Makoto Hasegawa [a,*], Yukari Yasuda [a], Makoto Tanaka [a], Kenya Nakata [b], Eri Umeda [b], Yanwen Wang [b], Chihiro Watanabe [b], Shoko Uetake [b], Tatsuki Kunoh [a], Masafumi Shionyu [a], Ryuzo Sasaki [a], Isamu Shiina [b,**], Tamio Mizukami [a]

[a] Faculty of Bioscience, Nagahama Institute of Bio-Science and Technology, 1266 Tamura-cho, Nagahama, Shiga 526-0829, Japan
[b] Department of Applied Chemistry, Faculty of Science, Tokyo University of Science, 1-3 Kagurazaka, Shinjuku-ku, Tokyo 162-8601, Japan

ARTICLE INFO

Article history:
Received 19 August 2013
Received in revised form
2 November 2013
Accepted 6 November 2013
Available online 16 November 2013

Keywords:
Proteasome inhibitors
Tamoxifen derivatives
Structure–activity relationship (SAR)
Docking studies

ABSTRACT

In a survey of nonpeptide noncovalent inhibitors of the human 20S proteasome, we found that a novel tamoxifen derivative, RID-F (compound **6**), inhibits all three protease activities of the proteasome at submicromolar levels. Structure–activity relationship studies revealed that a RID-F analog (RID-F-S*4, compound **25**) is the smallest derivative compound capable of inhibiting proteasome activity, with a potency similar to that of RID-F. Kinetic analyses of the inhibition mode and competition experiments involving biotin-belactosin A (a proteasome inhibitor) binding indicated that the RID-F derivatives interact with the protease subunits in a different manner. Culturing of human cells with these compounds resulted in accumulation of ubiquitinated proteins and induction of apoptosis. Thus, the RID-F derivatives may be useful lead chemicals for the generation of a new class of proteasome inhibitors.

1. Introduction

Eukaryotic cells have two different pathways for protein degradation: the lysosomal pathway and the ubiquitin-proteasome pathway. The lysosomal pathway breaks down endogenous and endocytosed exogenous proteins in a relatively nonspecific manner to provide amino acids as building materials for protein synthesis. In contrast, the ubiquitin-proteasome system is the major machinery for regulated proteolysis of endogenous proteins. Protein degradation by the ubiquitin-proteasome system is initiated by the labeling of targeted proteins with polyubiquitin chains in an intra- or extracellular signal-dependent manner [1]. Degradation of ubiquitinated proteins by the 26S proteasome plays a pivotal role in the regulation of a number of cellular processes, such as cell cycle progression, cell growth, proliferation, differentiation, apoptosis, gene transcription, and signal transduction [2]. Aberrant degradation of key regulatory proteins by the proteasome perturbs these processes, causing uncontrolled cell cycle progression and a decrease in cell death, both of which are hallmarks of tumorigenesis [3].

Several proteasome inhibitors have been proposed as anticancer drugs [1,4–8]. One of these inhibitors, the peptide boronate bortezomib, has been approved for the clinical treatment of multiple myeloma and mantle cell lymphoma [2]. The toxic boronate pharmacophore, however, causes severe side effects [9]. More recently, the tetrapeptide epoxyketone carfilzomib, which is an epoxomicin analog, has also been approved for the treatment of multiple myeloma [10–12]. In addition to being targeted in the treatment of various blood–borne tumors, proteasome inhibition has been suggested for the treatment of solid tumors [4], parasites, inflammation, immune diseases, and muscular dystrophies [13], encouraging development of new types of proteasome inhibitors with enhanced efficacy and fewer side effects [5].

The 26S proteasome is a large protein complex of ~2.5 MDa that consists of two subcomplexes with different functions: the 19S regulatory complex and the 20S catalytic core. The 20S catalytic core is a barrel-shaped protein composed of seven α subunits (α 1–7) and seven β subunits (β 1–7). The 19S regulatory complex also consists of multiple subunits and caps the 20S barrel at one or both ends. The 19S regulatory cap recognizes, unfolds, and translocates polyubiquitinated substrates into the 20S catalytic core, where the substrates are degraded. In the 20S proteasome core, the β1, β2, and β5 subunits act as proteases, with caspase-(peptidylglutamyl peptide hydrolase, PGPH), trypsin-, and chymotrypsin-like activities,

* Corresponding author. Tel.: +81 749 64 8114.
** Corresponding author. Tel.: +81 3 3260 4271.
E-mail addresses: m_hasegawa@nagahama-i-bio.ac.jp (M. Hasegawa), shiina@rs.kagu.tus.ac.jp (I. Shiina).

0223-5234/$ – see front matter © 2013 Elsevier Masson SAS. All rights reserved.
http://dx.doi.org/10.1016/j.ejmech.2013.11.009

respectively [1,2]. All of these hydrolytic activities are manifested through a threonine residue at the active site (Thr1).

Most of the dominant proteasome inhibitors, including bortezomib and carfilzomib, are short peptides that mimic substrates. The pharmacophores bound to the C-terminus of the peptide framework bind covalently to Thr1 in the 20S catalytic core active site. However, peptide bonds are easily degraded by endogenous proteases, and the reactive pharmacophores are susceptible to nucleophilic attack and are thus short-lived *in vivo*. Therefore, nonpeptide and noncovalent synthetic proteasome inhibitors would be valuable. More recently, a number of investigations have focused on inhibitors that are peptidic but noncovalent as part of efforts to overcome the drawbacks associated with covalent inhibitors [14]. These compounds include ritonavir [15], aminobenzylstatine [16], 3,4,5-trimethoxy-L-phenylalanine derivatives [17], 5-methoxy-1-indanone dipeptide benzamides [18], lipopeptides [19], N- and C-capped dipeptides derived from S-homophenylalanine [20,21], and TMC-95A [22,23] and its linear mimetic derivatives [24,25]. However, only a few inhibitors with both noncovalent and nonpeptidic characteristics have been reported [26].

Tamoxifen (TAM) binds to the estrogen receptor (ER) in place of the endogenous growth hormone, 17β-estradiol, suppressing proliferation of ER-positive breast cancer cells and inducing apoptosis [27]. However, it has been reported that TAM provokes apoptosis through an ER-independent pathway [28,29]. Indeed, TAM induces apoptosis of ER-negative cells through perturbation of the mitochondrial membrane potential [30]. Ridaifen-B (RID-B, see also Table 1), a TAM derivative, has been shown to induce apoptosis through the same pathway but with higher potency than TAM [30].

To find new noncovalent and nonpeptidic proteasome inhibitors, in this study we surveyed proteasome inhibition using a series of TAM derivatives. We found that RID-A, -B, -D, and -F inhibit the function of the 20S proteasome catalytic core *in vitro*. As RID-F was the most potent inhibitor of the three different enzymatic activities of the proteasome, we examined the structure–activity relationships of RID-F analogs with the hope of generating proteasome inhibitors that can be used to treat a wider range of diseases with minimal side effects.

2. Results and discussion

2.1. Synthesis of RID-F, RID-H, and other RID-F derivatives (RID-F-S*X)

Synthesis of RIDs A-H (compounds **1**–**8**) was conducted according to methods described in our previous reports and patents [31–35]. The synthetic pathways for producing new compounds **6** and **8**–**29** are depicted in Schemes 1–11. As an example, Scheme 1 illustrates the transformation of the phenol moieties of 1,1-bis(4-hydroxyphenyl)-2-phenylbut-1-ene into the corresponding aminoethyl ethers of RID-F (compound **6**) and RID-H (compound **8**) in dimethylformamide (DMF). 1,1-Bis(4-hydroxyphenyl)-2-phenylbut-1-ene was easily synthesized using a three-component coupling reaction involving

Table 1
Inhibition of human 20S proteasome activity by ridaifens (RIDs).

Compound number		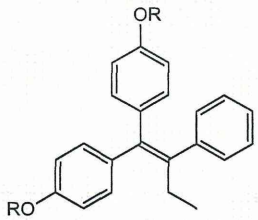	IC_{50} (μM)[a]		
			CT-L	T-L	PGPH
1	RID-A	R = $CH_2CH_2N(CH_3)_2$	3.36 ± 0.86	>10	2.99 ± 0.41
2	RID-B	R = 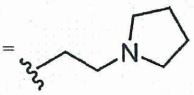	6.56 ± 0.14	>10	6.37 ± 0.28
3	RID-C	R = 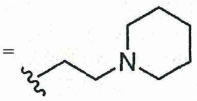	>10	>10	7.50 ± 0.18
4	RID-D	R = 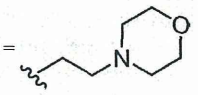	7.19 ± 0.28	>10	7.26 ± 0.27
5	RID-E	R = $CH_2CH_2N(C_2H_5)_2$	>10	>10	>10
6	RID-F	R = 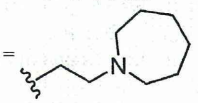	0.64 ± 0.14	0.34 ± 0.12	0.43 ± 0.08
7	RID-G	R = $CH_2CH_2CH_2N(CH_3)_2$	>10	NT	NT
8	RID-H	R = 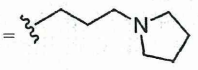	>10	NT	NT

[a] IC_{50} values denote concentrations of the compounds required for 50% inhibition of the activities (see "Experimental section"). Values are means of three experiments. CT-L, chymotrypsin-like activity; T-L, trypsin-like activity; PGPH, peptidylglutamyl peptide hydrolase activity. NT, not tested.

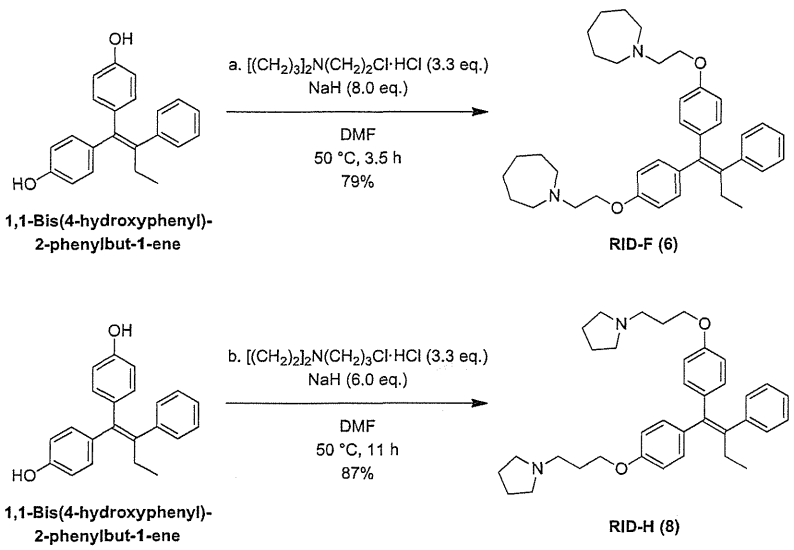

Reagents and conditions: (a) $[(CH_2)_3]_2N(CH_2)_2Cl{\cdot}HCl$ (3.3 eq.), NaH (8.0 eq.), DMF, 50 °C, 3.5 h, 79%; (b) $[(CH_2)_2]_2N(CH_2)_3Cl{\cdot}HCl$ (3.3 eq.), NaH (6.0 eq.), DMF, 50 °C, 11 h, 87%.

Scheme 1. Synthesis of RID-F (**6**) and RID-H (**8**) from 1,1-bis(4-hydroxyphenyl)-2-phenylbut-1-ene.

aromatic aldehyde, cinnamyltrimethylsilane, and anisole in the presence of $HfCl_4$ [31–33].

RID-F-S*3 (compound **24**), 1,1-bis{4-[2-(azepan-1-yl)ethoxy] phenyl}ethene, was synthesized from 4,4′-dihydroxybenzophenone (4,4′-DHBP) via a chemical approach involving *O*-alkylation, C1 segment installation, and acid-mediated dehydration, as shown in Scheme 2. First, the phenol moieties of 4,4′-DHBP were converted into the corresponding aminoethyl ethers with 85% yield by *O*-alkylation with *N*-(2-chloroethyl)hexahydro-1*H*-azepine HCl, and successive alkylation of the carbonyl group in RID-F-S*5 (compound **23**) using methyl Grignard reagent was carried out in tetrahydrofuran (THF) to produce the 1,1-diphenylethanol derivative RID-F-S*6 (compound **28**), with 88% yield. Finally, treatment of tertiary alcohol **28** with *p*-TsOH was attempted in benzene, and the facile

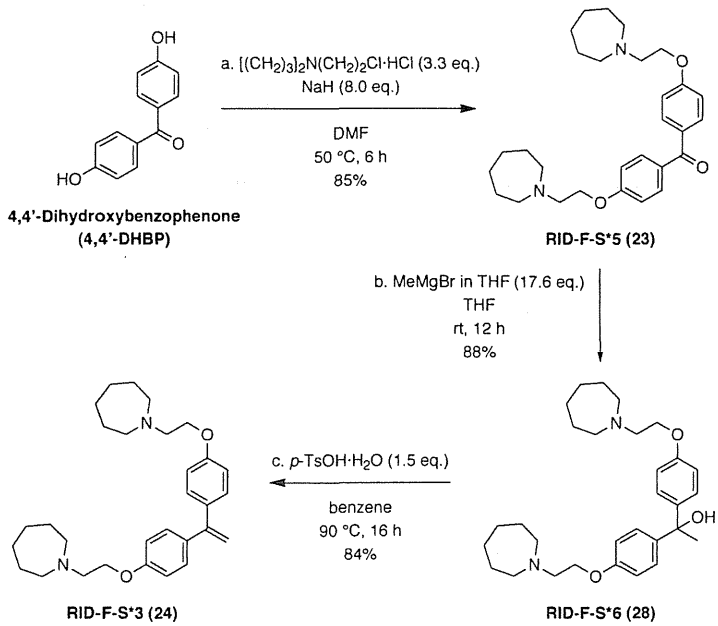

Reagents and conditions: (a) $[(CH_2)_3]_2N(CH_2)_2Cl{\cdot}HCl$ (3.3 eq.), NaH (8.0 eq.), DMF, 50 °C, 6 h, 85%; (b) MeMgBr in THF (1.12 M, 17.6 eq.), THF, room temperature, 12 h, 88%; (c) *p*-$TsOH{\cdot}H_2O$ (1.5 eq.), benzene, 90 °C, 16 h, 84%.

Scheme 2. Synthesis of RID-F-S*5 (**23**), RID-F-S*6 (**28**), and RID-F-S*3 (**24**) from 4,4′-dihydroxybenzophenone (4,4′-DHBP).

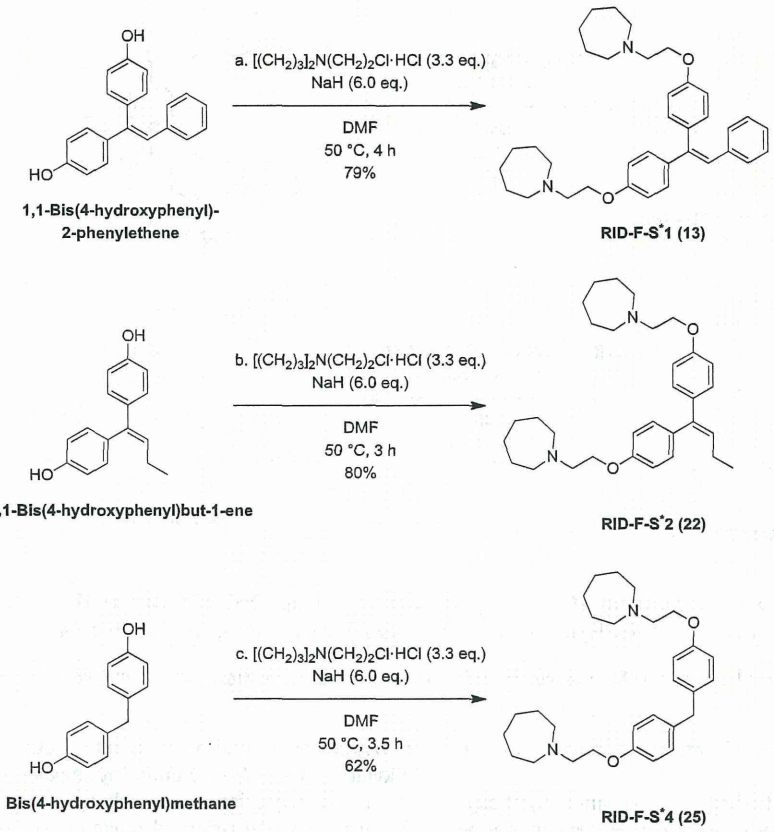

Reagents and conditions: (a) $[(CH_2)_3]_2N(CH_2)_2Cl{\cdot}HCl$ (3.3 eq.), NaH (6.0 eq.), DMF, 50 °C, 4 h, 79%; (b) $[(CH_2)_3]_2N(CH_2)_2Cl{\cdot}HCl$ (3.3 eq.), NaH (6.0 eq.), DMF, 50 °C, 3 h, 80%; (c) $[(CH_2)_3]_2N(CH_2)_2Cl{\cdot}HCl$ (3.3 eq.), NaH (6.0 eq.), DMF, 50 °C, 3.5 h, 62%.

Scheme 3. Synthesis of RID-F-S*1 (**13**), RID-F-S*2 (**22**), and RID-F-S*4 (**25**) from 1,1-bis(4-hydroxyphenyl)-2-phenylethene, 1,1-bis(4-hydroxyphenyl)but-1-ene, and bis(4-hydroxyphenyl)methane.

dehydration process resulted in successful synthesis of the desired molecule **24**, with 84% yield.

RID-F-S*13 (compound **9**), 1,1-bis{4-[2-(azepan-1-yl)ethoxy] phenyl}-2-cyclohexyl-2-phenylethene, was synthesized using the Mukaiyama reductive coupling reaction [36,37] depicted in Scheme 3. First, cyclohexyl phenyl ketone was treated with an excess of 4,4′-DHBP in the presence of the low-valent titanium species generated from titanium(IV) chloride with zinc powder in THF to afford 1,1-bis(4-hydroxyphenyl)-2-cyclohexyl-2-phenylethene, the desired olefin, with 65% yield. Next, the phenol moieties of the cross-coupling product were transformed into the corresponding aminoethyl ethers by *O*-alkylation in DMF, with 83% yield. Thus, an efficient method for the preparation of compound **9** was established through two steps from commercially available 4,4′-DHBP. RID-F-S*17 (compound **17**) and RID-F-S*24 (compound **16**) were also synthesized from 4,4′-DHBP with 6-undecanone or 7-tridecanone using the Mukaiyama reductive coupling reaction.

Other derivatives, RID-F-S*1 (compound **13**), RID-F-S*2 (compound **22**), RID-F-S*4 (compound **25**), RID-F-S*5 (compound **23**), RID-F-S*9 (compound **21**), RID-F-S*10 (compound **20**), RID-F-S*11 (compound **12**), RID-F-S*12 (compound **11**), RID-F-S*14 (compound **10**), RID-F-S*15 (compound **15**), RID-F-S*16 (compound **14**), RID-F-S*22 (compound **19**), RID-F-S*23 (compound **18**), RID-F-S*101 (compound **26**), RID-F-S*102 (compound **27**), and RID-F-S*103 (compound **29**) were synthesized from the corresponding commercially available bisphenols.

All RID physical properties (Mp, IR, ^1H and ^{13}C NMR, and HR-MS) are shown in the Supporting information.

2.2. Inhibition of proteasome activities by ridaifens

To identify new chemical moieties that function as proteasome inhibitors, we screened our in-house chemical libraries using an *in vitro* 20S proteasome inhibition assay. The potency of compounds was evaluated based on inhibition of the human 20S chymotrypsin-like (CT-L), trypsin-like (T-L), and PGPH activities of the 20S proteasome catalytic core. The IC_{50}, indicating the concentration required for 50% inhibition of the respective enzymatic activity (see Experimental section), was determined for each compound. The aldehyde proteasome inhibitor MG132 (Z-LLL-H) was used as a standard and had IC_{50} values of 0.011, 2.1, and 0.12 μM against CT-L, T-L, and PGPH activities, respectively. Of the 8 TAM derivatives tested (RID-A–RID-H; Table 1), RID-A, -B, and -D showed significant inhibition of CT-L and PGPH activities, but they did not significantly inhibit T-L activity. TAM did not inhibit any of the three enzymatic activities of the proteasome (Supplementary Table S1). RID-F, which has two homopiperidine moieties at the R positions, inhibited all three activities of the proteasome and was the most potent of the ridaifen compounds examined. The ridaifens did not inhibit calpain or cathepsin at concentrations of >10 μM (data not shown), which indicated that the ridaifens are highly specific inhibitors of the protease activities of the proteasome.

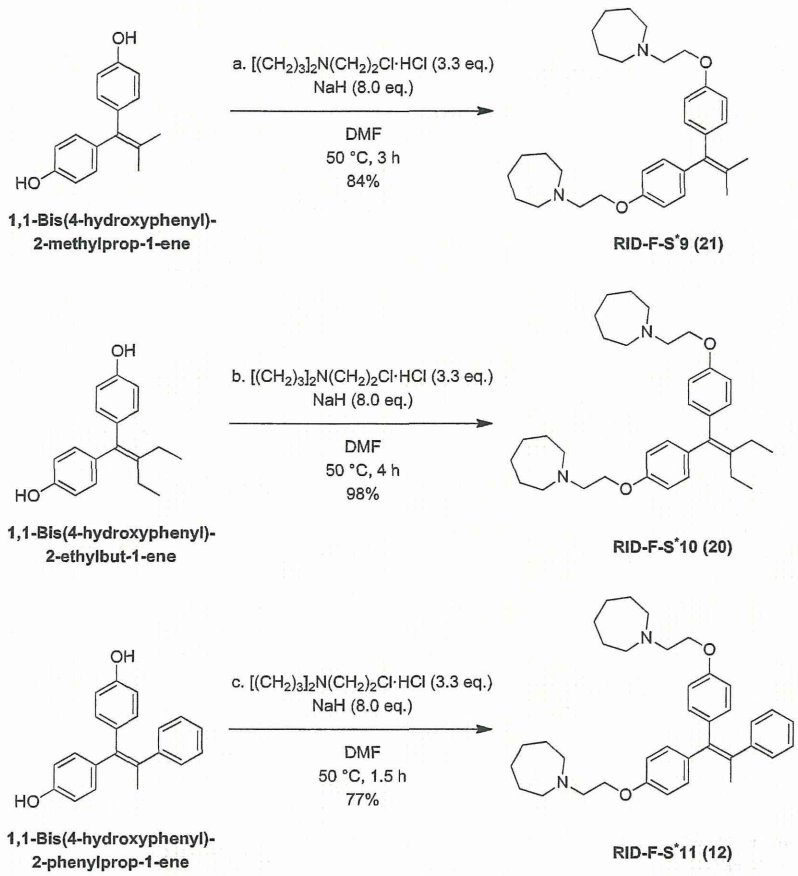

Reagents and conditions: (a) $[(CH_2)_3]_2N(CH_2)_2Cl{\cdot}HCl$ (3.3 eq.), NaH (8.0 eq.), DMF, 50 °C, 3 h, 84%; (b) $[(CH_2)_3]_2N(CH_2)_2Cl{\cdot}HCl$ (3.3 eq.), NaH (8.0 eq.), DMF, 50 °C, 4 h, 98%; (c) $[(CH_2)_3]_2N(CH_2)_2Cl{\cdot}HCl$ (3.3 eq.), NaH (8.0 eq.), DMF, 50 °C, 1.5 h, 77%.

Scheme 4. Synthesis of RID-F-S*9 (**21**), RID-F-S*10 (**20**), and RID-F-S*11 (**12**) from 1,1-bis(4-hydroxyphenyl)-2-methylprop-1-ene, 1,1-bis(4-hydroxyphenyl)-2-ethylbut-1-ene, and 1,1-bis(4-hydroxyphenyl)-2-phenylprop-1-ene.

2.3. Inhibition of proteasome activities by RID-F derivatives

Because RID-F blocked proteasomal protease activities at concentrations in the submicromolar range, we examined the structure–activity relationships of various RID-F derivatives. RID-F has an sp^2 carbon atom at the center position (X in Table 2). The side structure at the X position was substituted with different aromatic ring(s). Table 2 summarizes the structures and inhibitory activities of these RID-F derivatives. A comparison of inhibition potency (IC_{50}) against CT-L activity indicated that RID-F (**6**), RID-F-S*11 (**12**), and RID-F-S*1 (**13**) were the most potent compounds. It should be noted that the volume of the vinyl benzene side structure and the inhibition potency against CT-L, T-L, and PGPH activities were similar for all three compounds.

To examine the contribution of side structures of the RID-F derivatives to the inhibition potency, we compared the volumes of the derivatives with the pocket volume of the proteasome active site. Side-structure models were built with energy minimization and molecular dynamics using Chem3D software (PerkinElmer Inc.). The solvent-excluded volumes of the side structures of RID-F (**6**), RID-F-S*11 (**12**), and RID-F-S*1 (**13**) calculated using Connolly's program [38] in Chem3D software were 119, 102, and 84 $Å^3$, respectively. These values were close to the pocket volume (117 $Å^3$) of the PGPH active site of the yeast 20S proteasome β1 calculated using Pocket-Finder, which is based on the LIGSITE algorithm [39]. Compounds with side structures smaller than (RID-F-S*16 (**14**) and RID-F-S*15 (**15**)) or larger than vinyl benzene (RID-F-S*13 (**9**) and RID-F-S*14 (**10**)) demonstrated low inhibition potency. These data suggest that vinyl benzene is an optimally sized side structure for inhibiting proteasomal protease activity.

Next, the side structure at the X position was substituted with aliphatic linear chains of varying lengths. Table 3 summarizes the structures and proteasome inhibitory activities of this series of compounds. RID-F-S*24 (**16**), RID-F-S*17 (**17**), and RID-F-S*23 (**18**) have long hydrocarbon chains; the volumes of their side structures were calculated to be 235, 201, and 167 $Å^3$, respectively. These compounds demonstrated no inhibition of proteasome activity, indicating that hydrocarbon chains of more than eight carbon atoms in length interfere with the inhibitory activity of RID-F derivatives. RID-F-S*10 (**20**), RID-F-S*9 (**21**), RID-F-S*2 (**22**), RID-F-S*5 (**23**), and RID-F-S*3 (**24**), which have smaller and nonaromatic side structures, showed low inhibition potency.

To delineate the minimal structure necessary for proteasome inhibition, we examined a series of RID derivatives that had truncated side structures (Table 4). The smallest symmetric compound, RID-F-S*4 (**25**), demonstrated the highest inhibition potency, whereas, as seen with RID-F-S*110 (**30**) (Table 5) [40], removal of one of the two homopiperidine rings resulted in a critical loss of

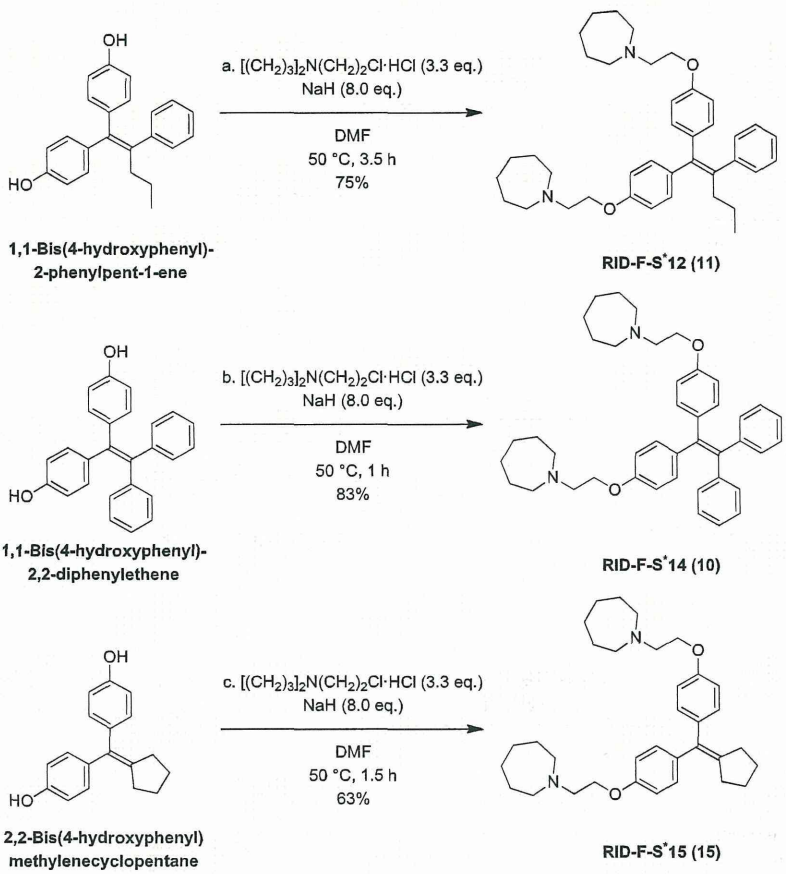

Reagents and conditions: (a) $[(CH_2)_3]_2N(CH_2)_2Cl{\cdot}HCl$ (3.3 eq.), NaH (8.0 eq.), DMF, 50 °C, 3.5 h, 75%; (b) $[(CH_2)_3]_2N(CH_2)_2Cl{\cdot}HCl$ (3.3 eq.), NaH (8.0 eq.), DMF, 50 °C, 1 h, 83%; (c) $[(CH_2)_3]_2N(CH_2)_2Cl{\cdot}HCl$ (3.3 eq.), NaH (8.0 eq.), DMF, 50 °C, 1.5 h, 63%.

Scheme 5. Synthesis of RID-F-S*12 (**11**), RID-F-S*14 (**10**), and RID-F-S*15 (**15**) from 1,1-bis(4-hydroxyphenyl)-2-phenylpent-1-ene, 1,1-bis(4-hydroxyphenyl)-2,2-diphenylethene, and 2,2-bis(4-hydroxyphenyl)methylenecyclopentane.

inhibition potency. Therefore, the structure of derivative RID-F-S*4 (**25**) appears to be the minimal structure possible for proteasome inhibition activity, and the presence of two homopiperidine rings appears to be crucial for inhibition.

2.4. Mode of RID-F derivative proteasome inhibition

Kinetic studies revealed that proteasome CT-L activity was inhibited by RID-F (**6**) in a noncompetitive manner, with a K_i of 0.58 ± 0.14 μM, whereas PGPH activity was inhibited in a competitive manner, with a K_i of 0.34 ± 0.22 μM (Fig. 1). The other RID-F derivatives exhibited similar inhibition of proteasome CT-L and PGPH activities; RID-F-S*14 (**10**) and RID-F-S*1 (**13**) inhibited CT-L activity noncompetitively, with K_i values of 1.10 ± 0.22 μM and 0.87 ± 0.32 μM, respectively, whereas they inhibited PGPH activity competitively, with K_i values of 1.02 ± 0.15 μM and 0.67 ± 0.29 μM, respectively (data not shown). It has been shown that substrates of PGPH activity inhibit CT-L activity and that this inhibition is caused by binding of PGPH substrates to a noncatalytic CT-L site(s) rather than through binding to an active site [11]. Taken together, from these data we inferred that RID-F and its derivatives bind to both the active PGPH site and a noncatalytic CT-L site(s), resulting in inhibition of CT-L activity. As described below, the results of docking simulations of ridaifens with the yeast counterpart of mammalian PGPH support this inference.

The chemical structures of the RID-F derivatives suggest that covalent binding to the proteasome is very unlikely. Indeed, labeling of proteasome subunits with a biotin-conjugated RID-F derivative failed to yield biotin-labeled proteins (data not shown). It has been shown that belactosin A preferentially inhibits both PGPH (β1 subunit) and CT-L (β5 subunit) by forming covalent linkages to the O^{γ} atom of the active site Thr1 [41]. Subunits covalently modified by biotin-labeled belactosin can be identified by Western blotting. Kinetic analyses showed that the RID-F derivatives inhibited PGPH activity in a competitive manner, suggesting direct interaction of the derivatives with the active site of the β1 subunit (Fig. 1B).

We then examined whether RID-F derivatives could impede covalent modification by biotin-labeled belactosin. In agreement with previous results [41], we found that biotin-belactosin A primarily bound β1 and β5 but also bound β2 with very low efficiency (Fig. 2). RID-F (**6**) and RID-F-S*4 (**25**) impeded binding of biotin-belactosin to β1 (PGPH activity) in a dose-dependent manner (Fig. 2A and B). Both compounds inhibited CT-L activity in a noncompetitive manner (Fig. 1A), and therefore we expected that they do not reduce binding of belactosin to β5 (CT-L activity). Contrary to this expectation, the compounds inhibited binding to